NEUTRON STAR INTERIOR COMPOSITION EXPLORER X-RAY TIMING OF THE RADIO AND γ-RAY QUIET PULSARS PSR J1412+7922 AND PSR J1849−0001

Slavko Bogdanov,[1] Wynn C. G. Ho,[2,3] Teruaki Enoto,[4] Sebastien Guillot,[5,6] Alice K. Harding,[7] Gaurava K. Jaisawal,[8] Christian Malacaria,[9,10] Sridhar S. Manthripragada,[11] Zaven Arzoumanian,[12] and Keith C. Gendreau[12]

[1] *Columbia Astrophysics Laboratory, Columbia University, 550 West 120th Street, New York, NY, 10027, USA*
[2] *Department of Physics and Astronomy, Haverford College, 370 Lancaster Avenue, Haverford, PA 19041, USA*
[3] *Mathematical Sciences, Physics and Astronomy, and STAG Research Centre, University of Southampton, Southampton SO17 1BJ, UK*
[4] *The Hakubi Center for Advanced Research and Department of Astronomy, Kyoto University, Kyoto 606-8302, Japan*
[5] *IRAP, CNRS, 9 avenue du Colonel Roche, BP 44346, F-31028 Toulouse Cedex 4, France*
[6] *Université de Toulouse, CNES, UPS-OMP, F-31028 Toulouse, France*
[7] *Astrophysics Science Division, NASA Goddard Space Flight Center, Greenbelt, MD 20771, USA*
[8] *National Space Institute, Technical University of Denmark, Elektrovej 327-328, DK-2800 Lyngby, Denmark*
[9] *NASA Marshall Space Flight Center, NSSTC, 320 Sparkman Drive, Huntsville, AL 35805, USA**
[10] *Universities Space Research Association, NSSTC, 320 Sparkman Drive, Huntsville, AL 35805, USA*
[11] *Instrument Systems and Technology Division, NASA Goddard Space Flight Center, Greenbelt, MD 20771, USA*
[12] *X-Ray Astrophysics Laboratory, NASA Goddard Space Flight Center, Greenbelt, MD 20771, USA*

ABSTRACT

We present new timing and spectral analyses of PSR J1412+7922 (Calvera) and PSR J1849−0001, which are only seen as pulsars in X-rays, based on observations conducted with the *Neutron Star Interior Composition Explorer* (*NICER*). We obtain updated and substantially improved pulse ephemerides compared to previous X-ray studies, as well as spectra that can be well-fit by simple blackbodies and/or a power law. Our refined timing measurements enable deeper searches for pulsations at other wavelengths and sensitive targeted searches by LIGO/Virgo for continuous gravitational waves from these neutron stars. Using the sensitivity of LIGO's first observing run, we estimate constraints that a gravitational wave search of these pulsars would obtain on the size of their mass deformation and r-mode fluid oscillation.

Keywords: pulsars: general — pulsars: individual (PSR J1412+7922, PSR J1849−0001) — stars: neutron — X-rays: stars — gravitational waves

1. INTRODUCTION

The vast majority of the ∼2600 known rotation-powered pulsars have been discovered and have had their spin parameters determined using observations at radio wavelengths (Manchester et al. 2005). However, an appreciable subset of pulsars in the Galaxy are observationally inaccessible in the radio due to severe dispersion/scattering or unfavorable viewing geometry such that the radio emission beams never intersect our line of sight. In addition, it is possible that some pulsars are intrinsically radio quiet. Regardless of the reason, sensitive observations for such objects at other wavelengths such as X-rays provide the only means of discovering them and characterizing their spin behavior.

The high Galactic latitude ($b = +37°$) X-ray source 1RXS J141256.0+792204 (also known as Calvera or PSR J1412+7922) was identified by Rutledge et al. (2008) and Shevchuk et al. (2009) as a strong neutron star candidate based on its soft X-ray spectrum and lack of optical counterpart. It was revealed with *XMM-Newton* to be a relatively nearby $P = 59.2$ ms pulsar with nearly sinusoidal pulsations (Zane et al. 2011). The X-ray emission from Calvera can be described by either a purely thermal spectrum or a composite thermal plus non-thermal model. Halpern et al. (2013) subsequently determined its period derivative to be $\dot{P} = (3.19 \pm 0.08) \times 10^{-15}$ s s^{-1}, which corresponds to char-

Corresponding author: Slavko Bogdanov
slavko@astro.columbia.edu

* NASA Postdoctoral Fellow

acteristic age $\tau_c \equiv P/2\dot{P} = 2.9 \times 10^5$ yr, spin-down luminosity $\dot{E} \approx 6 \times 10^{35}$ erg s^{-1}, and surface dipole magnetic field strength $B_s = 4.4 \times 10^{11}$ G. While these inferred properties are not unusual for a rotation-powered pulsar, radio searches have failed to detect pulsations down to fairly deep limits (>0.05 mJy; see Hessels et al. 2007; Zane et al. 2011). PSR J1412+7922 does not appear to be a γ-ray source either, despite its likely proximity ($D \lesssim 2$ kpc) and relatively high spin-down luminosity (Halpern 2011; Halpern et al. 2013). Based on these characteristics, this pulsar is speculated to be a possible descendant of the Central Compact Object (CCO) class, a population of enigmatic radio-quiet young neutron stars in supernova remnants (see, e.g., Gotthelf et al. 2013; De Luca 2017). Most recently, using *Chandra* HRC, Halpern & Gotthelf (2015) measured a proper motion for PSR J1412+7922 of $\mu = 69 \pm 26$ mas yr^{-1}, with a direction away from the Galactic plane.

The 38.5 ms X-ray pulsar PSR J1849−0001 was discovered in a targeted *Rossi X-ray Timing Explorer* (*RXTE*) observation of the soft γ-ray/TeV source IGR J18490−0000/HESS J1849−000 (Gotthelf et al. 2011). The measured spin-down rate $\dot{P} = 1.42 \times 10^{-14}$ s s^{-1} implies that PSR J1849−0001 is quite an energetic ($\dot{E} = 9.8 \times 10^{36}$ ergs s^{-1}) and young ($\tau_c = 42.9$ kyr) rotation-powered pulsar (Gotthelf et al. 2011; Kuiper & Hermsen 2015). The source exhibits a non-sinusoidal single pulse per rotation with width ~ 0.5 in rotation phase at both low energies (0.06–10 keV) and high energies (2–28 keV) and pulsed fractions of 0.77±0.04 and 0.88±0.08, respectively (also 0.76 ± 0.02 in the 2–10 keV band; Kuiper & Hermsen 2015). The hard non-thermal spectrum from a 23 ks 2012 *Chandra* ACIS-S observation can be fit with absorption $N_{\rm H} = (4.30 \pm 0.16) \times 10^{22}$ cm^{-2} and power law index $\Gamma = 1.08 \pm 0.02$. A 54 ks 2011 *XMM-Newton* spectrum can be fit with $N_{\rm H} = (4.5 \pm 0.1) \times 10^{22}$ cm^{-2} and $\Gamma \approx 1.2$ and yields a 2–10 keV unabsorbed flux $F_{2-10}^{\rm unabs} \approx 4.8 \times 10^{-12}$ ergs cm^{-2} s^{-1}, which implies X-ray luminosity $L_X = 2.8 \times 10^{34}$ ergs s^{-1} for an assumed distance of $D = 7$ kpc (Kuiper & Hermsen 2015; see also Vleeschower Calas et al. 2018, who analyzed the same data and obtain similar results). The ACIS-S data and a 25 ks 2011 HRC-S observation do not show evidence of extended emission from a pulsar wind nebula (PWN) at soft energies (0.1–2 keV and 0.5–2 keV, respectively) around PSR J1849−0001, but the ACIS-S data shows diffuse (2–10 keV) emission $\lesssim 30''$ in extent and several 0.5–10 keV point sources $\sim 1'$ from the pulsar. The 2011 *XMM-Newton* observation shows much fainter diffuse emission $75''$–$150''$ from PSR J1849−0001; this emission contributes 13% of the total flux around the pulsar and has a spectrum that can be fit by a power law with $\Gamma = 1.75\pm0.05$ (Kuiper & Hermsen 2015); note that Vleeschower Calas et al. (2018) find a larger diffuse contribution (23%), but this is likely due to different regions considered ($40''$–$100''$) and $N_{\rm H}$. Finally, we note

that *Fermi* LAT does not detect pulsed emission from PSR J1849−0001 (Abdo et al. 2013).

These two pulsars are of additional interest as potential sources of continuous gravitational waves (GWs) that may be detectable by the Laser Interferometer Gravitational-Wave Observatory (LIGO) and Virgo. Neutron stars can be sources of continuous GWs at 2 or $\approx 4/3$ times the pulsar spin frequency, depending on the GW emission mechanism, and stars with significant asymmetry and faster spin are stronger GW emitters (see, e.g., Glampedakis & Gualtieri 2017; Riles 2017). Previous GW searches of known pulsars used timing information from primarily radio and γ-ray observations (Aasi et al. 2014; Abbott et al. 2017a,b). Because PSR J1412+7922 and PSR J1849−0001 are only seen to be pulsed in X-rays, the timing models presented here will enable LIGO/Virgo to search for GWs from these two pulsars.

Herein we present X-ray studies of PSR J1412+7922 (Calvera) and PSR J1849−0001 using *NICER*. The paper is organized as follows. In Section 2, we present details of the observations and data reduction procedures. We present the X-ray timing analysis in Section 3 and spectral analysis in Section 4. We provide conclusions in Section 5.

2. OBSERVATIONS

NICER observations of a given target are typically carried out in segments lasting hundreds to $\sim$2000 seconds. All exposures of a target during the same UTC day are grouped into a single Observation ID (ObsID). The set of *NICER* observations of PSR J1412+7922 and PSR J1849−0001 analyzed here are summarized in Tables A1 and A2 of the Appendix. The *NICER* observations of these targets were often opportunistic, filling gaps in the schedule around higher-priority targets, such as transients. For PSR J1412+7922, the resulting data span 380 days from 2017 September 15 to 2018 October 3, while for PSR J1849−0001 the data span 223 days from 2018 February 13 to 2018 September 29.

3. TIMING ANALYSIS

Data processing and filtering were accomplished using HEASoft 6.24[1] and NICERDAS 2018-04-13_V004. The event data were first filtered to exclude any portions of the exposure accumulated during passages of the ISS through the South Atlantic Anomaly (SAA). For the purposes of producing event lists optimized for timing analysis, the data were further screened for instances of elevated count rates on a per detector basis, which revealed that detector 34 frequently showed count rates well above the median count rate of all active detectors. After excluding all events from this "hot" detector, a final pass was made to excise any time in-

---

[1] https://heasarc.nasa.gov/lheasoft/

Table 1. Timing Parameters of PSR J1412+7922 (Calvera).

Parameter	Value
Assumed parameters[a]	
R.A. (J2000.0)	$14^{\rm h}12^{\rm m}55\overset{\rm s}{.}867$
Decl. (J2000.0)	$+79°22'03\overset{''}{.}895$
$\mu_\alpha \cos\delta$ (mas yr^{-1})	$-40(30)$
μ_δ (mas yr^{-1})	$-56(21)$
Epoch of astrometric parameters (MJD)	$55,449.5$
Derived parameters	
Epoch (MJD TDB)	58150.46948
Period[b], P (ms)	59.199071070(18)
Period derivative[b], $\dot{P}$ (s s^{-1})	$3.29134(30) \times 10^{-15}$
Range of dates (MJD)	$58014.2 - 58394.1$
Spin-down luminosity, $\dot{E}$ (erg s^{-1})	6.3×10^{35}
Characteristic age, τ_c (kyr)	285
Surface dipole magnetic field, B_s (G) ...	4.5×10^{11}

[a] *Chandra* position and proper motion from Halpern & Gotthelf (2015).

[b] Tempo2 1σ uncertainties given in parentheses.

Table 2. Timing Parameters of PSR J1849−0001

Parameter	Value
Assumed parameters[a]	
R.A. (J2000.0)	$18^{\rm h}49^{\rm m}01\overset{\rm s}{.}632$
Decl. (J2000.0)	$-00°01'17\overset{''}{.}45$
Derived parameters	
Epoch (MJD TDB)	58239.916286135
Period[b], P (ms)	38.5222586295(19)
Period derivative[b], $\dot{P}$ (s s^{-1})	$1.415734(49) \times 10^{-14}$
Range of dates (MJD)	$58166.4 - 58355.9$
Spin-down luminosity, $\dot{E}$ (erg s^{-1}) ..	9.8×10^{36}
Characteristic age, τ_c (kyr)	43.1
Surface dipole magnetic field, B_s (G)	7.5×10^{11}

[a] *Chandra* position from Kuiper & Hermsen (2015).

[b] Tempo2 1σ uncertainties given in parentheses.

tervals of enhanced background affecting all detectors. This was done by constructing a light curve binned at 8 seconds and removing the time bins in which the count rate was in excess of 4.5 and 5.0 counts s^{-1} for PSR J1412+7922 and PSR J1849−0001, respectively, in the full *NICER* band (0.25–12 keV). These relatively high thresholds were selected in order to remove only peri-

ods strongly contaminated by background flaring. Using these filtering criteria, we obtained total clean exposures of 371.8 ks and 60.4 ks for the two sources for use in pulse timing analyses.

Since PSR J1412+7922 is known to be a soft thermal source, only events in the 0.3–3 keV range were considered in the timing analysis presented below. PSR J1849−0001, on the other hand, suffers from strong interstellar absorption ($N_H \approx 10^{22}$ cm^{-2}) so nearly all source emission is above ∼1 keV. Based on this, we selected only events in the 1–6 keV range for timing purposes. To correct for the telescope motion and make the transformation between Terrestrial Time (TT), used for the *NICER* event time stamps, and Barycentric Dynamical Time (TDB) we assumed the JPL DE421 solar system ephemeris. For both sources, as free pulsar parameters in the timing model we only consider the period P and period derivative $\dot{P}$. The sky positions for both pulsars were fixed at the values previously measured to sub-arcsecond precision with *Chandra*. Although PSR J1412+7922 has a measured proper motion, we only use it to correct for the resulting shift in position over time and do not fit for it.

Following standard pulsar timing procedures, we started by combining exposures taken on adjacent days to produce a single pulse time of arrival (TOA) measurement. The data were combined such that there is sufficient exposure to confidently detect the pulsar (typically 6-8 ks for both pulsars), while restricting the time span of each TOA to less then seven days. The ObsID
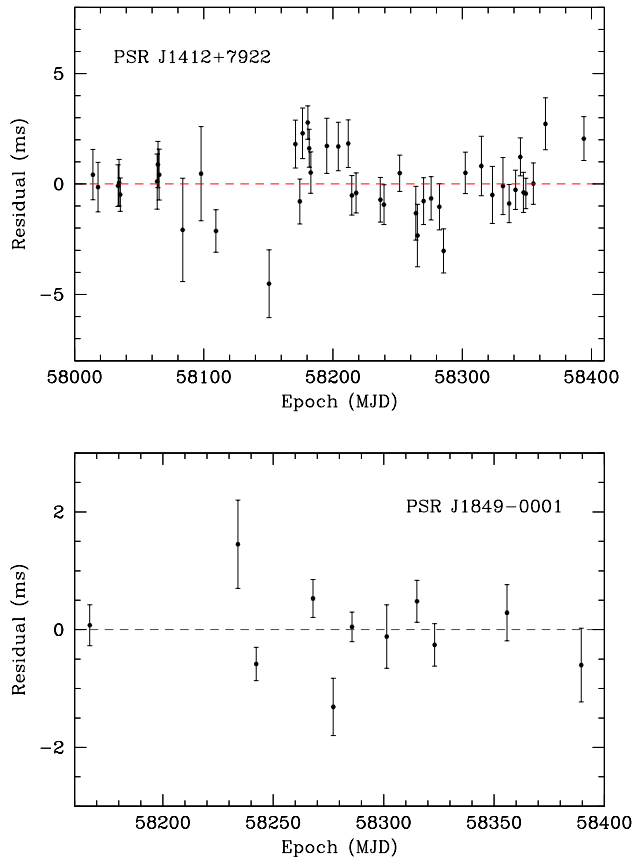
Figure 1. *NICER* timing residuals in milliseconds of PSRs J1412+7922 (top) and J1849−0001 (bottom) over the full observing time span for each source.

groupings of these TOAs are listed in the last column of Tables A1 and A2. This resulted in 44 and 11 *NICER* TOAs for PSR J1412+7922 and PSR J1849−0001, respectively. For both pulsars, we searched each ObsID grouping for pulsations around the known spin parameters to produce a folded and binned pulse profile at the detected periodicity. We fitted the profiles from the TOA where the pulsar is detected with the highest statistical significance (TOAs #16 and #3 for the two pulsars, respectively) as determined by the H-test (de Jager et al. 1989), with a single-peaked symmetric Gaussian template to determine the fiducial phase corresponding to the peak of the pulse (which we designate as $\phi = 0$). This template profile was used to generate a set of TOAs that were fit with a timing model using Tempo2 (Hobbs et al. 2006). In a final iteration, an improved template was generated using the entire refolded data set and with energy cuts that maximize the pulsation detection significance (0.37–1.97 keV for PSR J1412+7922 and 1.89–6 keV for PSR J1849−0001), photon phases were reassigned using the improved solution, and new TOAs were produced and refit to arrive at the final timing solution summarized in Tables 1 and 2. The
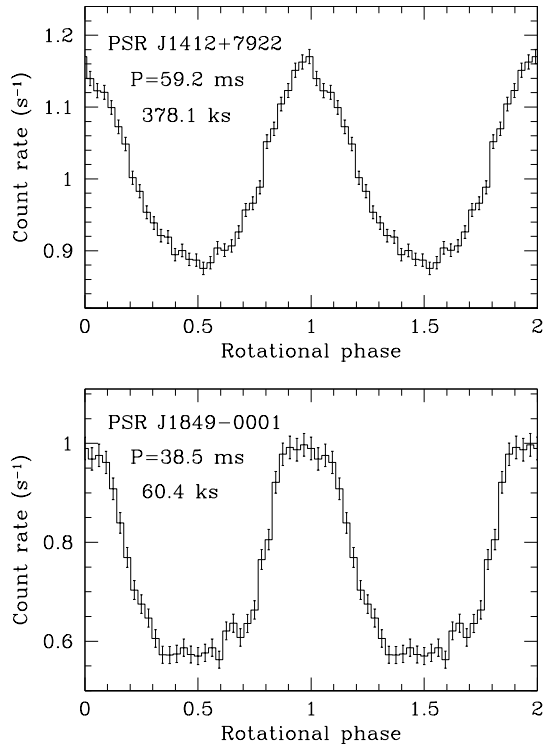

Figure 2. Pulse profiles of PSRs J1412+7922 in the 0.37–1.97 keV band (top) and J1849−0001 over 1.89–6 keV (bottom), folded at the ephemerides reported in Tables 1 and 2 using all available *NICER* data.

root mean square post-fit timing residuals for the two pulsars are 1.36 ms and 0.525 ms, respectively, which are the expected levels given the broad pulses. Adding a second period derivative ($\ddot{P}$) in the timing model for either pulsar does not result in a statistically significant improvement in the residuals and its value is consistent with zero.

The *NICER* timing residuals for PSR J1412+7922 and PSR J1849−0001 are shown in Figure 1, while the NICER pulse profiles of both pulsars folded using the new timing solutions are presented in Figure 2. The derived spin parameters (P and $\dot{P}$) for both pulsars are fully consistent with previous measurements but with substantially reduced uncertainties, with the values of $\dot{P}$ in particular being improved by two orders of magnitude. We note that some of the scatter evident in the TOA residuals may be due to unpredictable "timing noise" commonly seen in young pulsars.

4. SPECTRAL ANALYSIS

Figure 3 shows two-dimensional count maps versus pulse phase and energy for the two pulsars. These plots illustrate that PSR J1412+7922 is bright only in soft X-rays, while PSR J1849−0001 is relatively hard and detected in the higher energy band up to at least ∼6 keV. We carried out *NICER* spectral analyses with
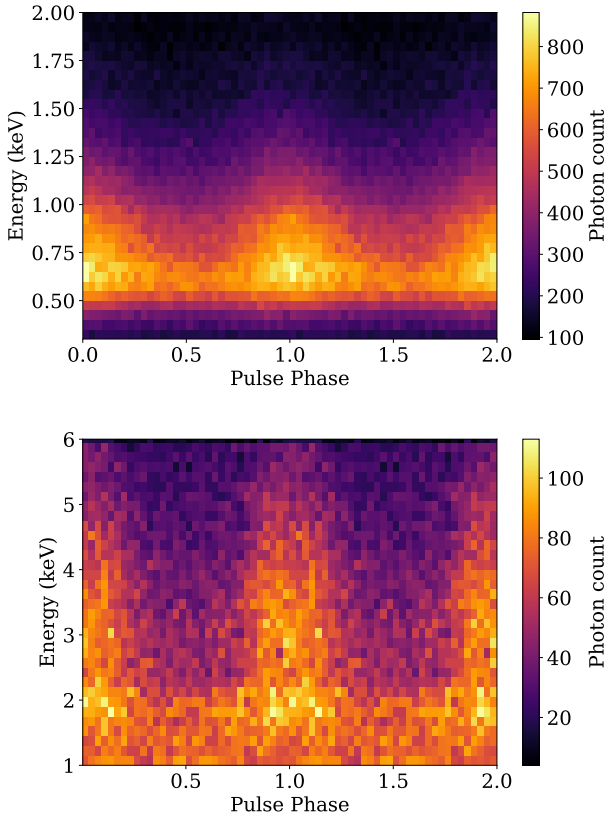
Figure 3. Photon counts as a function of pulse phase and energy for PSRs J1412+7922 (top) and J1849−0001 (bottom) folded at the ephemerides reported in Tables 1 and 2 using all available *NICER* data.

Figure 4. Spectral fitting of PSR J1412+7922 (Calvera, top panel) and PSR J1849−0001 (bottom panel). The two-temperature blackbody model is used for PSR J1412+7922, while the single power-law model is shown for PSR J1849−0001. See Tables 3 and 4 for the best fit parameters.

the calibration database (CALDB) version 20181105 and gain solution version `optmv7`. Cleaned events were extracted from Good Time Intervals (GTIs) defined by the standard filtering criteria, together with additional constraints based on a space-weather background model developed within the *NICER* team: KP < 5, where KP corresponds to the K_p geomagnetic activity index; COR_SAX > 1.914 × KP$^{0.684}$ + 0.25, where COR_SAX is the magnetic cut-off rigidity (in units of GeV/c); and FPM_UNDERONLY_COUNT < 200, where FPM_UNDERONLY_COUNT represents the rate of "undershoot" resets per enabled FPM per second, a measure of optical light-loading. In the following spectral studies, we do not use the filtering criteria to exclude time bins with high count rates described in §2. The corresponding background spectra are estimated using the space-weather background model and observations of seven "blank sky" fields adopted from *RXTE* studies (Jahoda et al. 2006). Three FPMs (DET_IDs 14, 34, and 54) are excluded from our spectral analyses because they sometimes exhibit higher background rates in the low-energy band compared to the other FPMs. We used a standard response matrix file (RMF; version 1.01) in
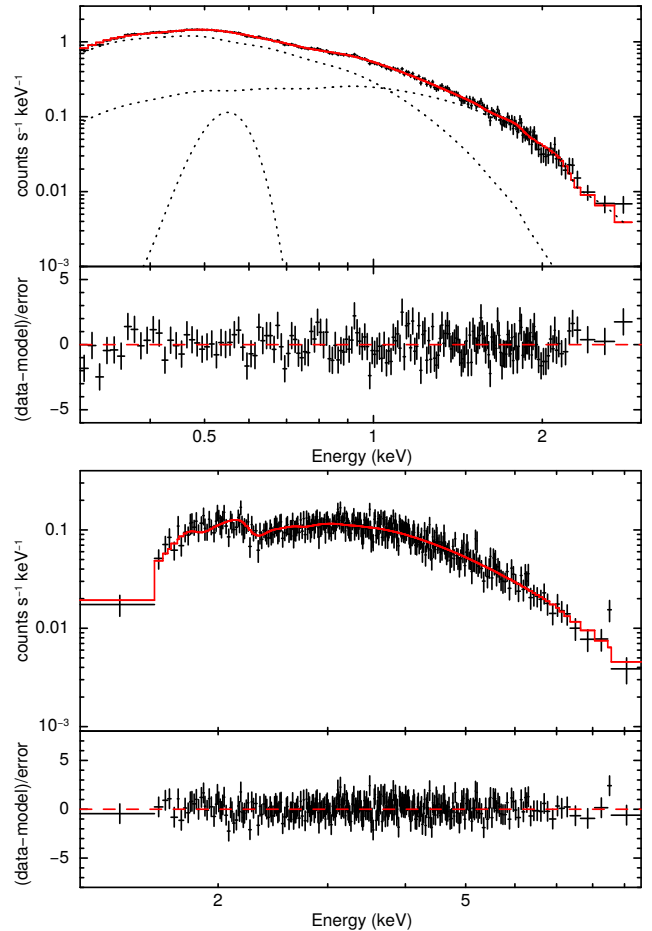
the CALDB and an ancillary response file (ARF) scaled to account for the three excluded detector modules.

We measure background-subtracted source count rates of 0.94 and 0.41 counts s^{-1} for PSR J1412+7922 (0.3–3.0 keV) and PSR J1849−0001 (1–10 keV), respectively. Derived spectra are binned so that individual bins have either > 4σ detection significance or up to 50 counts and 100 counts for PSR J1412+7922 and PSR J1849−0001, respectively. Figure 4 shows the data and best-fit spectral models for these two pulsars.

The soft X-ray bright source PSR J1412+7922 was detected below ∼2 keV (top panel of Figure 4). We performed fits of its spectrum in the 0.22–2.1 keV band with models that include photoelectric absorption (`tbabs` in XSPEC; Wilms et al. 2000) and two additional components, either two blackbodies (`bbodyrad+bbodyrad`) or a blackbody plus power-law (`bbodyrad+pegpwrlw`) because a single blackbody model can not reproduce the data; we note that Shibanov et al. (2016) obtain a

Table 3. Spectral Fit Parameters of PSR J1412+7922 (Calvera)

Component	Parameter	BB+PL	BB+BB
tbabs	$N_{\rm H}$ (10^{20} cm^{-2})	5.14 ± 0.31	0.29 ± 0.14
pegpwrlw (PL)	Γ	2.99 ± 0.06	$\cdots$
	Norm. (10^{-12} ergs s^{-1} cm^{-2}) [a]	0.11 ± 0.01	$\cdots$
bbodyrad (BB)	kT_1 (keV)	0.205 ± 0.003	0.154 ± 0.004
	R_1 (km) [b]	$1.01^{+0.04}_{-0.03}$	$2.21^{+0.08}_{-0.07}$
bbodyrad (BB)	kT_2 (keV)	$\cdots$	$0.319^{+0.013}_{-0.012}$
	R_2 (km) [b]	$\cdots$	0.37 ± 0.04
gabs	$E_{\rm c}$ (keV)	0.78 ± 0.02	0.76 ± 0.01
	σ (keV)	0.05 ± 0.02	0.08 ± 0.01
	strength[c]	0.008 ± 0.003	0.03 ± 0.01
$F^{\rm abs}_{0.3-3\,{\rm keV}}$ (10^{-13} erg cm^{-2} s^{-1})		9.5 ± 0.1	9.4 ± 0.2
χ^2/dof		$165.5/173$	$183.8/177$

[a] The normalization of the pegpwrlw model is given in units of 2–10 keV unabsorbed flux.

[b] Distance of 2 kpc assumed.

[c] The line strength is defined by $\sigma\tau\sqrt{2\pi}$, where τ is the optical depth.

good fit to rotation phase-averaged *Chandra* and *XMM-Newton* spectra using a single atmosphere model. Both sets of spectral models show fit residuals that can be modeled by an emission feature at $\sim$0.55 keV and an absorption feature at $\sim$0.76 keV. The former is thought to be a foreground feature due to solar wind charge exchange or a local hot bubble along the line of sight, but it could be related to a 0.5 keV emission feature reported in the *Chandra* spectrum (Shevchuk et al. 2009). We added a Gaussian emission model (gaussian) to take it into account. The latter absorption feature was previously seen in an *XMM-Newton* spectrum (Shibanov et al. 2016), and we find it in our *NICER* data to be phase-dependent with an energy shift over the pulse rotation. To account for it, we added a Gaussian absorption model (gabs in XSPEC). The best fit parameters are summarized in Table 3. Detailed phase-resolved spectral analysis with more realistic spectral models is the subject of ongoing work.

The $\sim$1.5–9 keV spectrum of PSR J1849−0001 (bottom panel of Figure 4) is well-fit by a photoelectric absorption model (tbabs) and either a single blackbody or power-law model. The best-fit parameters are listed in Table 4. We favor the power-law model, which was used in analyzing previous *RXTE* and *XMM-Newton* observations (Gotthelf et al. 2011; Kuiper & Hermsen 2015; Vleeschower Calas et al. 2018), because it is a better fit than the blackbody model, with an improvement of $\triangle\chi^2 = -31.9$, and the very high blackbody temperature is likely unrealistic. Our derived X-ray flux ($F^{\rm unabs}_{2-10} = (6.8 \pm 0.1) \times 10^{-12}$ erg cm^{-2} s^{-1}), ab-

sorption ($N_{\rm H} = 6.2 \times 10^{22}$ cm^{-2}), and photon index ($\Gamma = 1.54$) are different from previous *XMM-Newton* values ($F^{\rm unabs}_{2-10} \approx 4.8 \times 10^{-12}$ erg cm^{-2} s^{-1}, $N_{\rm H} = 4.5 \times 10^{22}$ cm^{-2}, and $\Gamma = 1.3$; Kuiper & Hermsen 2015). However, as discussed in Section 1, there is notable diffuse emission around the pulsar due to its PWN, and the non-imaging detectors of *NICER* cannot resolve these two components.

5. CONCLUSIONS

We presented new X-ray timing and spectroscopic analyses of the X-ray-only pulsars PSRs J1412+7922 and J1849−0001 based on *NICER* data. We obtain phase-connected timing solutions spanning 380 and 223 days for the two pulsars, respectively. The *NICER* timing campaigns enable a two orders of magnitude improvement in the spin-down rate measurements compared to previous studies of the two pulsars.

The LIGO Scientific Collaboration and Virgo Collaboration perform targeted searches of known pulsars whose accurately measured position and spin properties reduce the parameter space for GW searches. With an accurate timing model, phase-coherent GW searches can be performed over long periods of time, thereby maximizing the potential for detection. Past targeted searches primarily used timing models obtained by radio telescopes and *Fermi* to place constraints on GW emission from some 200 radio and γ-ray pulsars (Abbott et al. 2017a; see also Aasi et al. 2014; Abbott et al. 2017b).

The GW strain amplitude $h_0(\nu_{\rm GW})$ that is produced at GW frequency $\nu_{\rm GW}$ ($= 2\nu$, where $\nu = 1/P$) by

Table 4. Spectral Fit Parameters of PSR J1849−0001

Component	Parameter	PL	BB
`tbabs`	N_{H} (10^{22} cm^{-2})	$6.23^{+0.27}_{-0.26}$	$3.23^{+0.17}_{-0.16}$
`pegpwrlw` (PL)	Γ	1.54 ± 0.07	$\cdots$
	Norm. (10^{-12} ergs s^{-1} cm^{-2}) [a]	$6.75^{+0.12}_{-0.11}$	$\cdots$
`bbodyrad` (BB)	kT (keV)	$\cdots$	1.43 ± 0.04
	R(km) [b]	$\cdots$	0.254 ± 0.011
	$F^{\mathrm{abs}}_{0.3-3\,\mathrm{keV}}$ (10^{-12} erg cm^{-2} s^{-1})	$5.14^{+0.11}_{-0.15}$	$4.30^{+0.09}_{-0.10}$
	χ^2/dof	225.4/309	257.3/309

[a] The normalization of the `pegpwrlw` model is given in units of 2–10 keV unabsorbed flux.

[b] Distance of 7 kpc assumed.

a quadrupolar mass deformation with ellipticity $\varepsilon \equiv |I_{xx} - I_{yy}|/I_{zz}$, where I_{xx}, I_{yy}, and I_{zz} are the triaxial components of the stellar moment of inertia, is (see, e.g., Aasi et al. 2014)

$$h_0 = \frac{16\pi^2 G}{c^4}\frac{\varepsilon I_{zz}}{D}\nu^2$$
$$= 4.23 \times 10^{-26}\left(\frac{1\,\mathrm{kpc}}{D}\right)\left(\frac{\varepsilon}{10^{-4}}\right)\left(\frac{\nu}{10\,\mathrm{Hz}}\right)^2. \quad (1)$$

For the dominant r-mode fluid oscillation of dimensionless amplitude α, $\nu_{\mathrm{GW}} \approx 4\nu/3$ (Andersson et al. 2014; Idrisy et al. 2015; Jasiulek & Chirenti 2017) and the equivalent GW strain amplitude h_0 (see, e.g., Owen 2010) is

$$h_0 \sim 5.36 \times 10^{-26}\alpha\left(\frac{1\,\mathrm{kpc}}{D}\right)\left(\frac{\nu}{10\,\mathrm{Hz}}\right)^3. \quad (2)$$

An upper bound on the GW strain that can be produced by a pulsar with known ν and $\dot{\nu}$ ($= -\dot{P}/P^2$) is obtained by assuming that the pulsar rotational energy loss is due entirely to GW emission (i.e., neglecting electromagnetic losses). In such an idealized case, the "spindown limit" on GW strain for a quadrupolar mass deformation is

$$h_{\mathrm{sd}} = \left(-\frac{5G}{2c^3}\frac{I_{zz}}{d^2}\frac{\dot{\nu}}{\nu}\right)^{1/2}$$
$$= 2.55 \times 10^{-25}\left(\frac{1\,\mathrm{kpc}}{D}\right)$$
$$\times \left(\frac{10\,\mathrm{Hz}}{\nu}\right)^{1/2}\left(\frac{-\dot{\nu}}{10^{-12}\,\mathrm{Hz\,s^{-1}}}\right)^{1/2}, \quad (3)$$

while the spin-down limit for a r-mode fluid oscillation is 3/2 that given by equation (3) (Owen 2010). Thus, as GW searches become more sensitive (pushing the measured h_0 to lower values, such that $h_0 < h_{\mathrm{sd}}$), the con-

straint on ellipticity improves as

$$\varepsilon = 6.03 \times 10^{-4}\left(\frac{10\,\mathrm{Hz}}{\nu}\right)^{5/2}\left(\frac{-\dot{\nu}}{10^{-12}\,\mathrm{Hz\,s^{-1}}}\right)^{1/2}\left(\frac{h_0}{h_{\mathrm{sd}}}\right). \quad (4)$$

Similarly, the constraint on r-mode amplitude is

$$\alpha = 7\left(\frac{10\,\mathrm{Hz}}{\nu}\right)^{7/2}\left(\frac{-\dot{\nu}}{10^{-12}\,\mathrm{Hz\,s^{-1}}}\right)^{1/2}\left(\frac{h_0}{h_{\mathrm{sd}}}\right). \quad (5)$$

For an assumed (maximum) distance of 2 kpc to PSR J1412+7922 (Halpern et al. 2013; Halpern & Gotthelf 2015), we find that the GW spindown limit is $h_{\mathrm{sd}} = 9.51 \times 10^{-26}$. For an assumed distance of 7 kpc to PSR J1849−0001 (Gotthelf et al. 2011), we find $h_{\mathrm{sd}} = 6.98 \times 10^{-26}$. These h_{sd} can be approximately compared to the estimated GW strain sensitivity $h_0(\nu_{\mathrm{GW}})$ of the LIGO O1 run given in Abbott et al. (2017a); in particular, $h_0(23\,\mathrm{Hz}) \approx 3 \times 10^{-25}$, $h_0(34\,\mathrm{Hz}) \approx 9 \times 10^{-26}$, and $h_0(52\,\mathrm{Hz}) \approx 4 \times 10^{-26}$. Thus O1 data is at or two times the spindown limit for PSR J1412+7922 and is lower than the spindown limit for PSR J1849−0001. The timing models obtained from *NICER* data and presented here enable future GW observations to obtain constraints for each X-ray pulsar. For example, a GW search at O1 sensitivity would limit the ellipticity of both PSR J1412+7922 and PSR J1849−0001 at $\varepsilon < 1 \times 10^{-4}$ and, for PSR J1849−0001, r-mode amplitude at $\alpha < 0.7$ and GW contribution to the pulsar's rotational energy loss at $< 30\%$. Of course, future GW searches will have greatly improved sensitivities (see, e.g., Abbott et al. 2018), such that much stronger limits will be achieved. While neither pulsar has been seen to glitch, glitch activity is known to correlate with age (e.g., Fuentes et al. 2017). Young pulsars also tend to exhibit spin fluctuations (timing noise), which only contemporaneous observations can track. Thus it is important to continue monitoring these relatively young pulsars in X-rays (and other X-ray-only pulsars) with *NICER* to

maintain the accuracy of each timing model in order to complement GW searches.

APPENDIX

A. LOG OF *NICER* OBSERVATIONS OF PSR J1412+7922 AND PSR J1849−0001

The set of *NICER* observations of PSR J1412+7922 and PSR J1849−0001 are summarized in Tables A1 and A2, respectively. The tables list the ObsIDs, the start time of the exposure in UTC units, the good exposure time after excluding intervals during SAA passage, and the TOA number in which the observation was included for the timing analysis.

Facilities: NICER

Software: Tempo2 (Hobbs et al. 2006)

REFERENCES

Aasi, J., Abadie, J., Abbott, B. P., et al. 2014, ApJ, 785, 119

Abbott, B. P., Abbott, R., Abbott, T. D., et al. 2017a, ApJ, 839, 12

—. 2017b, PhRvD, 96, 122006

—. 2018, Living Reviews in Relativity, 21, 3

Abdo, A. A., Ajello, M., Allafort, A., et al. 2013, ApJS, 208, 17

Andersson, N., Jones, D. I., & Ho, W. C. G. 2014, MNRAS, 442, 1786

de Jager, O. C., Raubenheimer, B. C., & Swanepoel, J. W. H. 1989, A&A, 221, 180

De Luca, A. 2017, in Journal of Physics Conference Series, Vol. 932, Journal of Physics Conference Series, 012006

Fuentes, J. R., Espinoza, C. M., Reisenegger, A., et al. 2017, A&A, 608, A131

Glampedakis, K., & Gualtieri, L. 2017, ArXiv e-prints, arXiv:1709.07049

Gotthelf, E. V., Halpern, J. P., & Alford, J. 2013, ApJ, 765, 58

Gotthelf, E. V., Halpern, J. P., Terrier, R., & Mattana, F. 2011, ApJL, 729, L16

Halpern, J. P. 2011, ApJL, 736, L3

Halpern, J. P., Bogdanov, S., & Gotthelf, E. V. 2013, ApJ, 778, 120

Halpern, J. P., & Gotthelf, E. V. 2015, ApJ, 812, 61

Hessels, J. W. T., Stappers, B. W., Rutledge, R. E., Fox, D. B., & Shevchuk, A. H. 2007, A&A, 476, 331

Hobbs, G. B., Edwards, R. T., & Manchester, R. N. 2006, MNRAS, 369, 655

Idrisy, A., Owen, B. J., & Jones, D. I. 2015, PhRvD, 91, 024001

Jahoda, K., Markwardt, C. B., Radeva, Y., et al. 2006, ApJS, 163, 401

Jasiulek, M., & Chirenti, C. 2017, PhRvD, 95, 064060

Kuiper, L., & Hermsen, W. 2015, MNRAS, 449, 3827

Manchester, R. N., Hobbs, G. B., Teoh, A., & Hobbs, M. 2005, AJ, 129, 1993

Owen, B. J. 2010, PhRvD, 82, 104002

Riles, K. 2017, Modern Physics Letters A, 32, 1730035

Rutledge, R. E., Fox, D. B., & Shevchuk, A. H. 2008, ApJ, 672, 1137

Shevchuk, A. S. H., Fox, D. B., & Rutledge, R. E. 2009, ApJ, 705, 391

Shibanov, Y., Danilenko, A., Zharikov, S., Shternin, P., & Zyuzin, D. 2016, ApJ, 831, 112

Vleeschower Calas, L., Kaufmann, S., Alvarez Ochoa, C., & Tibolla, O. 2018, arXiv e-prints, arXiv:1802.04833

Wilms, J., Allen, A., & McCray, R. 2000, ApJ, 542, 914

Zane, S., Haberl, F., Israel, G. L., et al. 2011, MNRAS, 410, 2428

Table A1. Log of *NICER* observations of PSR J1412+7922

Observation ID	Start time (UTC)	Exposure (s)	TOA Number
1020290101	2017-09-15T00:03:43	2329	1
1020290102	2017-09-18T05:03:20	4072	1
1020290103	2017-09-19T07:16:00	726	1
1020290104	2017-09-20T03:19:20	1256	1
1020290105	2017-09-21T08:56:55	2521	2
1020290106	2017-09-22T04:42:58	5693	2
1020290107	2017-10-07T07:29:20	10070	3
1020290108	2017-10-08T02:02:40	10399	4
1020290109	2017-10-08T23:34:40	18025	5
1020290110	2017-10-10T00:16:17	6426	6
1020290111	2017-11-06T22:27:00	221	6
1020290112	2017-11-06T23:51:04	7983	7
1020290113	2017-11-08T00:42:00	6540	8
1020290114	2017-11-25T17:05:40	268	9
1020290115	2017-11-26T16:06:40	1006	9
1020290116	2017-11-26T23:50:00	533	9
1020290117	2017-12-10T08:26:04	962	10
1020290118	2017-12-11T04:33:00	436	10
1020290119	2017-12-21T19:27:36	338	11
1020290120	2017-12-22T02:54:17	9258	11
1020290121	2018-02-01T11:05:14	3650	12
1020290122	2018-02-21T00:23:20	6154	13
1020290123	2018-02-22T07:17:33	2214	13
1020290124	2018-02-23T09:28:40	3154	14
1020290125	2018-02-24T16:25:00	2147	14
1020290126	2018-02-25T03:15:00	1040	14
1020290127	2018-02-26T00:50:00	2817	14
1020290128	2018-02-27T05:50:40	7033	15
1020290129	2018-03-03T01:11:40	14462	16
1020290130	2018-03-04T03:10:00	11346	17
1020290131	2018-03-05T01:06:00	7839	18
1020290132	2018-03-06T00:15:40	1796	18
1020290133	2018-03-17T22:57:33	821	19
1020290134	2018-03-18T00:30:10	5450	19
1020290135	2018-03-26T01:34:40	2163	20
1020290136	2018-03-27T00:42:16	4741	20
1020290137	2018-03-31T23:41:00	461	21
1020290138	2018-04-01T18:14:40	480	21
1020290139	2018-04-02T00:24:00	3198	21
1020290140	2018-04-03T18:06:00	629	21
1020290141	2018-04-04T17:05:00	778	21
1020290142	2018-04-05T00:58:20	2915	21
1020290143	2018-04-06T00:06:40	8892	22
1020290144	2018-04-07T00:49:40	6788	23
1020290145	2018-04-08T02:49:20	1514	23
1020290146	2018-04-09T11:10:20	818	23

Table A1 continued

Bogdanov et al.

Table A1 *(continued)*

Observation ID	Start time (UTC)	Exposure (s)	TOA Number
1020290147	2018-04-10T19:37:38	856	23
1020290148	2018-04-11T11:07:37	419	23
1020290149	2018-04-12T07:17:20	374	23
1020290150	2018-04-27T00:34:39	6866	24
1020290151	2018-04-28T13:31:40	329	24
1020290152	2018-05-01T00:17:37	12147	25
1020290153	2018-05-13T05:23:17	14394	26
1020290154	2018-05-22T22:17:37	478	27
1020290155	2018-05-23T01:22:58	1342	27
1020290156	2018-05-24T02:04:54	1120	27
1020290157	2018-05-26T03:25:40	1387	27
1020290158	2018-05-27T01:03:20	3954	28
1020290159	2018-05-28T00:13:00	3183	29
1020290160	2018-05-29T00:55:00	1001	29
1020290161	2018-06-01T01:25:20	1287	29
1020290162	2018-06-02T02:13:20	2053	29
1020290163	2018-06-03T13:47:00	1468	30
1020290164	2018-06-04T02:07:35	796	30
1020290165	2018-06-05T02:49:35	1287	30
1020290166	2018-06-06T20:24:43	1681	30
1020290167	2018-06-07T05:53:13	426	30
1020290168	2018-06-08T01:57:14	4238	30
1020290169	2018-06-09T02:37:33	1767	31
1020290170	2018-06-10T04:58:19	2928	31
1020290171	2018-06-13T06:56:00	1941	31
1020290172	2018-06-13T23:55:20	2161	31
1020290173	2018-06-15T16:04:20	620	32
1020290174	2018-06-16T04:25:40	5708	32
1020290175	2018-06-17T02:02:40	2841	32
1020290176	2018-07-02T03:10:20	4201	33
1020290177	2018-07-03T05:23:00	5897	33
1020290178	2018-07-04T13:45:40	739	33
1020290179	2018-07-12T17:33:00	346	34
1020290180	2018-07-15T19:41:40	1429	34
1020290181	2018-07-17T01:06:20	3690	34
1020290182	2018-07-20T04:45:40	895	35
1020290183	2018-07-23T15:52:00	436	35
1020290184	2018-07-24T07:19:00	495	35
1020290185	2018-07-26T17:58:38	1731	35
1020290186	2018-07-27T01:41:38	1681	35
1020290187	2018-07-28T08:33:00	824	36
1020290188	2018-07-28T23:55:40	2910	36
1020290189	2018-08-01T11:17:42	1751	36
1020290190	2018-08-03T15:53:00	580	37
1020290191	2018-08-05T09:56:20	1016	37
1020290192	2018-08-06T07:34:00	1780	37
1020290193	2018-08-07T21:47:56	1328	37
1020290194	2018-08-08T00:52:56	7480	37

Table A1 continued

Table A1 *(continued)*

Observation ID	Start time (UTC)	Exposure (s)	TOA Number
1020290195	2018-08-09T07:48:59	956	38
1020290196	2018-08-10T20:53:33	1324	38
1020290197	2018-08-10T23:58:52	3082	38
1020290198	2018-08-12T00:38:40	6129	38
1020290199	2018-08-13T01:22:53	6696	39
1020290201	2018-08-14T23:34:19	610	39
1020290202	2018-08-15T01:06:59	2480	39
1020290203	2018-08-16T14:07:40	2469	39
1020290204	2018-08-17T00:57:59	9688	40
1020290205	2018-08-18T04:50:59	9448	41
1020290206	2018-08-19T01:00:01	10341	41
1020290207	2018-08-23T03:44:00	354	42
1020290208	2018-08-24T00:04:59	2252	42
1020290209	2018-08-25T00:33:00	4883	42
1020290210	2018-08-26T01:28:20	1832	42
1020290211	2018-08-29T07:51:20	3708	43
1020290212	2018-09-03T08:33:20	1084	43
1020290213	2018-09-04T19:59:40	1544	43
1020290214	2018-10-02T00:32:59	3882	44
1020290215	2018-10-03T01:16:16	6154	44

Table A2.   Log of *NICER* observations of PSR J1849−0001

Observation ID	Start time (UTC)	Exposure (s)	TOA Number
1020660101	2018-02-13T23:49:40	187	1
1020660102	2018-02-14T01:22:20	504	1
1020660103	2018-02-15T03:38:40	978	1
1020660104	2018-02-16T02:45:20	1333	1
1020660105	2018-02-17T00:49:28	1486	1
1020660106	2018-02-19T06:35:00	896	1
1020660107	2018-02-20T10:30:17	980	1
1020660108	2018-02-21T05:09:40	498	1
1020660109	2018-03-22T04:11:20	188	⋯
1020660110	2018-03-24T08:34:58	677	⋯
1020660113	2018-04-21T08:17:58	1176	2
1020660115	2018-04-26T01:01:20	319	2
1020660116	2018-05-01T21:53:40	351	3
1020660117	2018-05-02T01:01:40	746	3
1020660118	2018-05-03T00:08:20	2481	3
1020660119	2018-05-04T00:50:00	5489	3
1020660120	2018-05-05T09:16:00	1442	3
1020660121	2018-05-06T00:43:40	34	3
1020660122	2018-05-22T18:12:20	866	4
1020660123	2018-05-23T01:55:20	3985	4
1020660124	2018-05-24T16:45:20	152	4
1020660126	2018-05-29T22:54:49	545	4
1020660127	2018-05-30T00:27:29	2678	4
1020660128	2018-06-01T00:19:30	2250	5
1020660129	2018-06-02T04:36:00	210	5
1020660130	2018-06-06T22:54:00	558	5
1020660131	2018-06-08T05:38:40	145	5
1020660132	2018-06-12T01:57:16	1898	6
1020660133	2018-06-15T18:00:37	1387	6
1020660134	2018-06-16T00:20:40	1406	6
1020660135	2018-06-17T01:03:40	4147	6
1020660136	2018-06-18T01:34:40	3007	6
1020660137	2018-06-19T00:44:20	1533	6
1020660138	2018-06-24T09:38:00	252	7
1020660139	2018-06-25T05:43:20	595	7
1020660140	2018-06-26T20:23:20	105	7
1020660141	2018-06-27T04:04:20	1691	7
1020660142	2018-06-28T07:54:00	262	7
1020660143	2018-07-02T09:14:40	147	7
1020660144	2018-07-03T08:23:20	423	7
1020660145	2018-07-10T03:50:40	72	⋯
1020660146	2018-07-12T03:42:52	1933	8
1020660147	2018-07-13T13:54:00	371	8
1020660148	2018-07-14T03:28:41	1397	8
1020660149	2018-07-15T02:49:40	832	8
1020660150	2018-07-16T03:22:20	2096	8
1020660151	2018-07-19T16:38:29	994	8
1020660153	2018-07-22T18:21:40	984	9
1020660154	2018-07-24T01:22:21	5167	9
1020660155	2018-08-21T15:02:35	2142	10
1020660156	2018-08-25T22:35:57	985	10
1020660157	2018-08-26T00:08:37	288	10
1020660158	2018-09-26T20:50:23	748	11
1020660159	2018-09-26T23:55:43	1057	11
1020660160	2018-09-28T11:28:37	587	11
1020660161	2018-09-29T02:55:39	79	11